

Can the Stephani model be an alternative to FRW accelerating models?

Włodzimierz Godłowski¹ & Jerzy Stelmach² & Marek Szydłowski¹

October 19, 2018

1. Astronomical Observatory of the Jagiellonian University, 30-244 Krakow, Orla 171, Poland

2. Institute of Physics, University of Szczecin, Wielkopolska 15, 70-451 Szczecin, Poland e-mail: jerzy.stelmach@univ.szczecin.pl

Abstract

A class of Stephani cosmological models as a prototype of non-homogeneous universe is considered. The non-homogeneity can lead to accelerated evolution which is now observed from the SNIa data. Three samples of type Ia supernovae obtained by Perlmutter *et al.*, Tonry *et al.* and Knop *et al.* are taken into account. Different statistical methods (best fits as well as maximum likelihood method) to obtain estimates of the model parameters are used. Stephani model is considered as an alternative to the concordance of Λ CDM model in the explanation of the present acceleration of the universe. The model explains the acceleration of the universe at the same level of accuracy as the Λ CDM model (χ^2 statistics are comparable). From the best fit analysis it follows that the Stephani model is characterized by higher value of density parameter Ω_{m0} than the Λ CDM model. It is also shown that the obtained results are consistent with location of CMB peaks.

1 Introduction

In the paper of Stelmach and Jakacka [1] it was suggested that the effect of acceleration of the universe can be driven by non-homogeneities in the

Stephani model [2, 3]. We perform the statistical verification of this hypothesis using current available astronomical data. We use three different samples of supernovae where Perlmutter sample [4] is treated as the fiducial data set. For comparison both the Tonry *et al.* [5] (improved by Barris *et al.* [6]) and Knop *et al.* [7] are used.

To find which model fits to the data in the best way we use the χ^2 statistics. The parameters of the models are estimated using the maximum likelihood method. One-dimensional probability distribution function (pdf) over model parameters is presented to deepen statistical insight.

Recently found accelerated expansion of our Universe [8] is explained in the literature by the presence of the Λ -term or the so-called quintessence matter satisfying the equation of state with negative pressure [9]. Observation of type Ia supernovae (SN Ia) revealed that this form of energy called dark energy could dominate the present evolution of the universe. Therefore it is important to consider different candidates for dark energy. In the paper of Stelmach and Jakacka it was shown that non-homogeneity in spherically symmetric Stephani model can be treated as some kind of dark energy due to which the universe accelerates (we call this model ‘‘S-J model’’). It is a sort of fictitious fluid for which density parameter Ω_{non} can be defined. Then dynamics can be formally reduced to the FRW flat model with additional fluid satisfying the equation of state $p = (-2/3)\rho$ corresponding to the equation of state for topological defects in a form of domain walls [10, 11, 12].

The best fitting procedure applied to supernovae data as well as confidence level for the redshift-magnitude relation shows that Ω_{non} should dynamically dominate the present evolution of the Universe if we want to explain observational data without cosmological term (see also [13]).

2 Stephani Model in the S-J version

Stephani model in the S-J version can be described by the generalized Friedman equation [1]

$$\dot{R}^2 + k = \frac{A^2}{R^{1+3\alpha}}, \quad (1)$$

where $k(t) = \beta R(t)$ is an effective curvature index which depends on time. β and α are constants ($p = \alpha\rho$). In the above equation non-homogeneity is not explicitly present. This is due to the choice of the time parameter.

Equation (1) is de facto a first integral of the Einstein equation which is a second order equation for the scale factor. It is obtained by assuming that the observer is placed at a symmetry center $p(r \approx 0, t) = \alpha\rho(t)$. We consider the universe in the neighbourhood of this center.

The relation

$$k(t) = \beta R(t), \quad (2)$$

is a special form of a more generalized ansatz of a type

$$k(t) = \beta R^\gamma(t), \gamma = \text{const.} \quad (3)$$

However, $\gamma = 1$ is a simplest case, and our goal is to show that such exotic model can explain SN Ia data of Perlmutter even in this simple case.

For further purposes it is convenient to write down Eq. (1) in a dimensionless form

$$\dot{x}^2 = \sum_{i=0}^1 \Omega_{i,0} x^{-(3\alpha_i+1)}, \quad (4)$$

where $x \equiv R/R_0$ is the so-called radius of the universe in units R_0 . Here the differentiation is carried out over the dimensionless time parameter $\tau \equiv |H_0|t$. The parameters Ω_{i0} ($i = 0, 1$) are defined

$$\Omega_{i0} = \frac{\rho_{i0}}{3H_0^2}, \quad (5)$$

where the subscript 0 means that a quantity with this subscript corresponds to the present epoch

$$\rho_{i0} \equiv \rho_i(x = 1). \quad (6)$$

In our model $\alpha_0 \equiv \alpha$ and $\alpha_1 \equiv -2/3$ like for topological defects, hence

$$\rho_\alpha \equiv \frac{C_\alpha}{R^{3+3\alpha}}, \quad \text{and} \quad \rho_{\text{non}} \equiv \frac{(-3\beta)}{R}, \quad (7)$$

where C_α is some constant.

In the given parametrization our non-homogeneous Stephani model looks formally as a flat Friedman model with two noninteracting components.

3 Stephani model as a hamiltonian system

Because of interpretation of the S-J model in terms of FRW model with additional fictious fluid we can simply find hamiltonian formalism for dynamics of the system. A first integral of the Friedman equation can always be used for reduction of the motion of the system to a motion of a particle of unit mass in one dimensional potential [14]. If we define

$$\rho_{\text{eff}} \equiv \sum_i \rho_i(R) = f(R), \quad (8)$$

then the potential is

$$V(R) \equiv -\frac{\rho_{\text{eff}}}{6} R^2 = \frac{\beta}{2} R - \frac{A^2}{2} \frac{1}{R^{1+3\alpha}} \quad (9)$$

and the Euler-Lagrange equation of motion reads

$$\ddot{R} = -\frac{\partial V}{\partial R} \quad (10)$$

and has a Newton-like form.

The Hamiltonian in the considered case has the form:

$$\mathcal{H} = \frac{P_R^2}{2} + V(R), \quad (11)$$

where we defined $P_R \equiv \dot{R}$

Trajectories of the system lie on a zero energy level $\mathcal{H} = 0$ and a hamiltonian constraint must coincide with the form of the first integral of the equation of motion (10).

The advantage of having the hamiltonian function given by Eq (11) is that one is then able to make easily full classification of solutions in the configuration space [1]. Moreover dynamics can be presented in two dimensional phase plane.

The corresponding equations of motion describe a simple dynamical system consisting of a particle moving in one dimensional potential:

$$\dot{x} = y,$$

$$\dot{y} = -\frac{\partial V}{\partial x}, \quad (12)$$

where $x = R$, $y = \dot{R}$ and $V(x)$ is given by (9), and $y^2/2 + V(x) = 0$ is its first integral. Qualitative analysis of differential equation implies a shift from finding and analysing individual solution to investigating the space of all solutions. Certain properties (such as existence or absence of horizons, existence of singularities) are believed to be realistic if they can be attributed to a larger class of models within the space of all solutions (phase space).

This approach offers a possibility of investigating the space of all possible solutions for the considered problem. Of course the system (12) possesses the first integral $\mathcal{H} = 0$ which defines a family of algebraic curves (phase curves) on which the trajectories of the system lie. The phase portrait of the considered system for a) $\alpha = 0$ (dust) is shown in Fig. 1 and for b) $\alpha = 1/3$ (radiation) in Fig. 2.

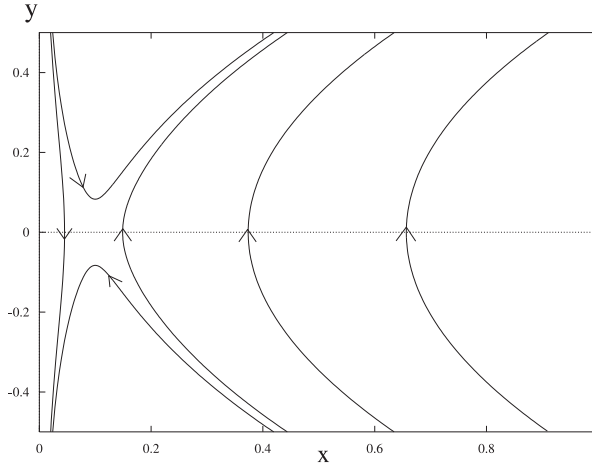


Figure 1: Phase portrait of S-J model for dust.

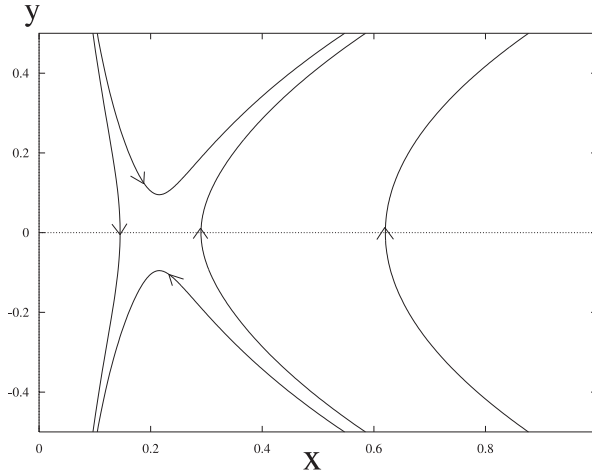


Figure 2: Phase portrait of S-J model for radiation.

The system is described by the equations $\dot{x} = y$, $\dot{y} = -\partial V/\partial x$ and the first integral is $y^2/2 + V(x) = 0$, where $V(x) = (1/2)(\beta x - A^2/x^{1+3\alpha})$ and we put $\beta = -1$. The phase domain is $x > 0$. The acceleration region is situated to the right of the saddle point, therefore for the Lemaitre-Eddington (loitering) universes the acceleration begins in the middle of a quasi-static stage.

For comparison the FRW model with dust and cosmological constant is presented in Fig. 3. We can observe how non-homogeneity term can mimic cosmological constant term. In the particular cases we have: a) $\dot{x} = y$, $\dot{y} = -(1/2)(\beta x + A^2/x^2)$, b) $\dot{x} = y$, $\dot{y} = -(1/2)(\beta + A^2/x^3)$, where $A = 0.1$, $\beta = -1$, c) $\dot{x} = y$, $\dot{y} = -(\Lambda/3)x - \rho_0/6x^2$, where $\Lambda = 0.7$, $\rho_0 = 0.3$ with $V(x) = -(\Lambda/3)x^2 - \rho_0/6x$.

The phase portrait is organized by critical points (x_0, y_0) (i.e singular

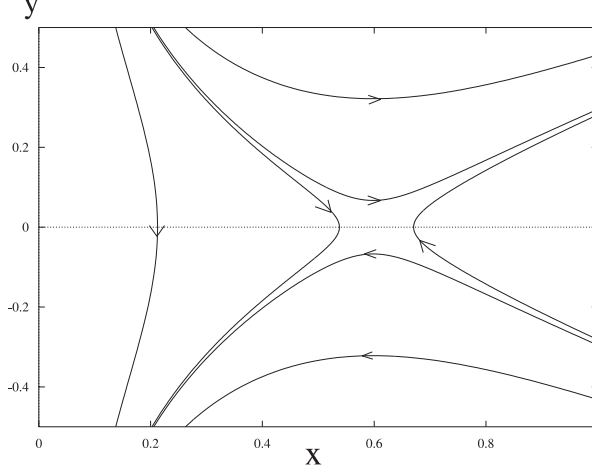


Figure 3: Phase portrait of FRW model with dust and cosmological constant.

solution for which $y_0 = 0$ and $\partial V/\partial x|_{(x_0, y_0)} = 0$) and joining them trajectories. Hence the phase portrait provides a global qualitative picture for the dynamics. Two phase portraits are equivalent if there exists an orientation preserving homeomorphism mapping integral curves of the systems. In our case the critical point for $\beta + (1 + 3\alpha) < 0$ is representing by static universe. Then

$$y_0 = 0, \quad x_0 = \left(-\frac{\beta}{(1 + 3\alpha)} A^2 \right)^{-\frac{1}{(2+3\alpha)}}, \quad (13)$$

where $\beta/(1 + 3\alpha) < 0$. While constructing the phase portrait it is important for the system to be linearized near the critical points because the Hartman-Grobman theorem says that the original system is equivalent to its linear part in the nearby hyperbolic critical points (a critical point is hyperbolic (non-degenerate)) if there exists such i that $\text{Re}\lambda_i \neq 0$, where λ_i are eigenvalues of a linearization matrix. A character of critical points is determined by characteristic equation for the linearization matrix

$$A = \begin{pmatrix} 0, & 1 \\ -\frac{\partial^2 V}{\partial x^2}, & 0 \end{pmatrix}_{(x_0, y_0=0)}. \quad (14)$$

Since in our case $\text{Tr}A = 0$ only saddle points ($\partial^2 V/\partial x^2|_{(x_0, 0)} < 0$) or centres ($\partial^2 V/\partial x^2|_{(x_0, 0)} > 0$) are admissible.

After some simple calculations one can check that a type of the critical point depends on the diagram of the potential, namely:

$$\det A = \frac{\partial^2 V}{\partial x^2}|_{(x_0, 0)} = -\frac{1}{2} A^2 (1 + 3\alpha) (2 + 3\alpha) R_0^{-3(1+\alpha)}. \quad (15)$$

Therefore for $\alpha > 1/3$ there exists only one critical point which is of saddle type, i.e it is a structurally stable point. The full knowledge of the dynamical system comprises also its behaviour at infinity. To achieve this one usually transforms the phase space into a Poincaré sphere. Then infinitely distant points of the phase plane are mapped onto the sphere's equator. The phase trajectories are mapped into corresponding curves on S^2 . The character of critical points is preserved and new critical points representing asymptotic states of the system can appear at the equator. Then an orthogonal projection of any hemisphere onto a tangent plane compactifies phase portrait.

4 Horizon and flatness problem

Due to existence of the first integral in such a system we can discuss some interesting properties of the evolutionary path. There is a theorem [15] about nonexistence of particle horizon in such a model, namely if $R \rightarrow 0$ and $\dot{R} < C$, where C is a constant, then there is no particle horizon in the past. In terms of potentials, if $V(R) \rightarrow \text{constant}$ for $R \rightarrow 0$ then there exists no particle horizon. It follows from the implication

$$\dot{R} \leq C \Rightarrow V \geq -\frac{C^2}{2}. \quad (16)$$

We can see from Fig. 1 and Fig. 2 in the S-J paper that all models with exception of case a) do not possess particle horizons. This is equivalent to nonexistence of the horizon problem in the corresponding models. However, it does not necessarily mean that if the condition $\dot{R} < C$ for $R \rightarrow 0$ is not satisfied then the horizon problem appears. In that case explicit evaluation of the integrals is required. We shall not deal with the problem in the present paper.

As regards a flatness problem it does not appear in a cosmological model if for later times the curvature term does not dominate the matter term. In our model for the the problem not to appear we need the following condition to be satisfied

$$|\beta R(t)| = |k(t)| \leq \frac{A^2}{|R^{1+3\alpha}(t)|}. \quad (17)$$

Hence

$$\alpha \leq -\frac{2}{3}.$$

Of course this is not the case considered either in the S-J or in the present paper, hence the flatness problem must be solved in a similar way as in the standard cosmology (e.g. using inflationary scenario).

5 Acceleration

The case $\beta < 0$ is particularly interesting because the corresponding cosmological model without matter ($A = 0$) evolves with constant acceleration. With matter it accelerates always for later times independently of α . It follows from the relation

$$\ddot{R} = -\frac{\partial V}{\partial R} = \frac{1}{2}\beta - \frac{A^2}{2}(1 + 3\alpha)R^{-3\alpha-2}. \quad (18)$$

Let us now differentiate both sides of the Eq. (4) with respect to τ

$$\ddot{x} = -\frac{1}{2} \sum_{i=0}^1 (1 + 3\alpha_i) \Omega_{i0} x^{-(3\alpha_i+2)}. \quad (19)$$

If we want the model to accelerate at the present epoch we must put $\ddot{x} > 0$ at $x = 1$. Hence we get the expected result

$$\Omega_{\text{non}0} > \Omega_{\alpha 0}, \quad (20)$$

since this is the nonhomogeneity, which drives the acceleration.

6 Magnitude-redshift relation

It is well known that luminosity of observed objects, depends sensitively on the spatial geometry (curvature) and dynamics of the Universe. Therefore a cosmic distance measure, e.g. luminosity distance, depends on the present densities of different components filling up the universe and their equations of state. For this reason, the magnitude-redshift relation is proposed as a potential test for cosmological models and play important role in determining cosmological parameters [16].

Let us consider an observer located at $r = 0$ and at the moment $t = t_0$ receiving light emitted at t from the source of absolute luminosity L located at the radial distance r . Cosmological redshift z of the source is related to t and t_0 by the formula

$$\frac{1+z}{V(r,t)} = \frac{R(t_0)}{R(t)}, \quad (21)$$

where the function $V(r, t)$ is

$$V(r, t) = 1 + \frac{1}{4}\beta R(t)r^2. \quad (22)$$

If the apparent luminosity of the source measured by the observer is l , then the luminosity distance d_L of the source, defined

$$l = \frac{L}{4\pi d_L^2}, \quad (23)$$

is given by:

$$d_L = \frac{(1+z)R_0 r}{V(r, t)}. \quad (24)$$

For historical reasons, the observed and absolute luminosities are defined respectively in terms of K -corrected observed and absolute magnitudes m and M ($l = 10^{-2m/5} \times 2.52 \times 10^{-5} \text{erg cm}^{-2} \text{s}^{-2}$, $L = 10^{-2M/5} \times 3.02 \times 10^{35} \text{erg s}^{-2}$) [17]. When written in terms of m and M , Eq.(23) yields

$$m(z, \mathcal{M}, \Omega_{\alpha 0}) = \mathcal{M} + 5 \log_{10}[\mathcal{D}_L(z, \Omega_{\alpha 0})], \quad (25)$$

where

$$\mathcal{M} = M - 5 \log_{10} H_0 + 25 \quad (26)$$

and

$$\mathcal{D}_L((z, \Omega_{\alpha 0}) \equiv H_0 d_L((z, \Omega_{\alpha 0}, H_0) \quad (27)$$

is a dimensionless luminosity distance in Mpc.

The radial coordinate r in the expression (22) for d_L can be found by evaluation of the integral

$$r = \frac{1}{R_0 H_0} \int_x^1 \frac{dy}{\sqrt{\Omega_{\alpha 0} y^{1-3\alpha} + (1 - \Omega_{\alpha 0}) y^3}}, \quad (28)$$

where $x \equiv R/R_0$. Since in order to compare with observations the apparent luminosity m must be a function of the redshift z , the x parameter should be calculated from the relation

$$z(x) = \frac{1}{x} - 1 + \frac{\Omega_{\alpha 0} - 1}{4} \left[\int_x^1 \frac{dy}{\sqrt{\Omega_{\alpha 0} y^{1-3\alpha} + (1 - \Omega_{\alpha 0}) y^3}} \right]^2. \quad (29)$$

which follows from (21). Of course in a general case to find x analytically is not an easy task. Formally we have to find an inverse function $x(z)$. The problem of finding $d_L(z)$ must be solved numerically and the simplest way to do that is to regard the function $d_L(z)$ as given in a parametric representation

$$d_L(x) = \frac{1}{x H_0} \sqrt{\frac{4[z(x) + 1 - 1/x]}{\Omega_{\alpha 0} - 1}}, \quad (30)$$

and $z(x)$ is given by (29).

Similarly as in the paper of Jakacka and Stelmach we consider physically the simplest case, i.e. we assume that in the neighbourhood of the symmetry center the matter filling up the universe is a dust, hence $\alpha = 0$. We define $\Omega_{m0} \equiv \Omega_{\alpha 0}|_{\alpha=0}$. In this case the expression (29) takes a form

$$z(x) = \frac{1}{x} - 1 + \frac{\Omega_{m0} - 1}{4} \left[\int_x^1 \frac{dy}{\sqrt{\Omega_{m0}y + (1 - \Omega_{m0})y^3}} \right]^2 \quad (31)$$

($\Omega_{\text{non}0} = 1 - \Omega_{m0}$), which can be evaluated using Weierstrass elliptic function \mathcal{P} [14]. The invariants g_2 and g_3 determining \mathcal{P} function are

$$g_2 = \frac{1}{4}\Omega_{m0}(\Omega_{m0} - 1), \quad g_3 = 0.$$

Accuracy of the fit is characterized by the parameter

$$\chi^2 = \sum_i \frac{(m_{0,i}^{\text{obs}} - m_{0,i}^{\text{theor}})^2}{\sigma_{m,i}^2 + \sigma_{z,i}^2}, \quad (32)$$

where $m_{0,i}^{\text{obs}}$ is the measured value, $m_{0,i}^{\text{theor}}$ is the value calculated in the model described above, $\sigma_{m,i}^2$ is a measurement error of m , while $\sigma_{z,i}^2$ is a measurement error of z following from the dispersion in peculiar velocities of galaxies.

We assume that supernovae measurements come with uncorrelated Gaussian errors and in this case the likelihood functions \mathcal{L} can be determined from chi-squared statistics $\mathcal{L} \propto \exp(-\chi^2/2)$ [4, 18].

7 Results of the statistical analysis with the Perlmutter sample.

In the paper of Stelmach and Jakacka it was shown that spherically symmetric Stephani cosmological model satisfying natural assumptions concerning local equation of state for the matter may explain supernovae data of Perlmutter in the context of the magnitude-redshift relation. In the present paper we discuss this problem in more detail and we find numerical values of these parameters such that observational data are best fitted to our theoretical $m - z$ curve. We take the whole sample of Perlmutter (all 60 galaxies) into account not rejecting any. Separately we analyse the sample of 54 supernovae (Perlmutter sample C), where 4 outliers and 2 reddened supernovae were excluded, finding no significant differences. In Fig. 4 we present plots

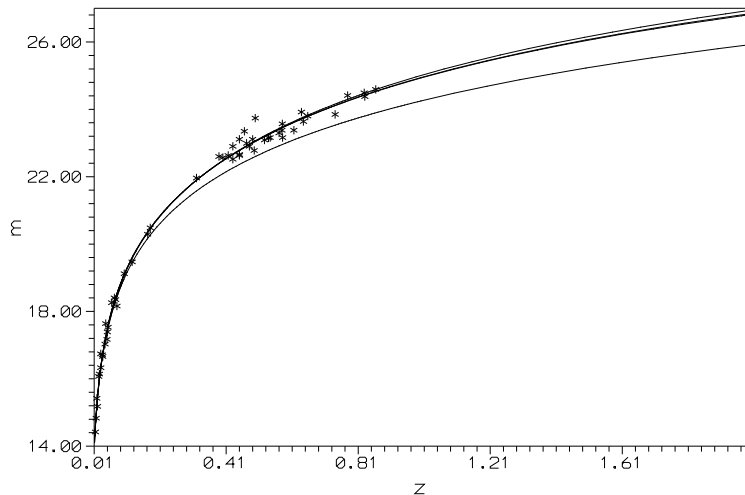


Figure 4: The Redshift-magnitude relation for Stephani model (Perlmutter Sample A).

of magnitude-redshift relations for the Stephani model and the Perlmutter sample A.

The lower line corresponds to standard Einstein-de Sitter model, the line in the middle to our spherically symmetric Stephani model, i.e. $\mathcal{M} = -3.37$, $\Omega_{m0} = 0.40$ (this line is inseparable from the Λ CDM (Perlmutter) model with $\Lambda = 0.7$ and $\Omega_{m0} = 0.3$), the upper line to Stephani model with $\Omega_{m0} = 0.3$. From Fig. 4 we can see that the Perlmutter model and our best fit model are indistinguishable on the basis of the present available data.

In Table 1 we present results of analysis with \mathcal{M} obtained as a best fit for "classical" Perlmutter model with $\Omega_{m0} = 0.3$, $\Omega_{\Lambda0} = 0.7$ (top line for each samples) and with marginalization over \mathcal{M} (second line for each samples). The best fit has been obtained using Bayes technique. For $\mathcal{M} = -3.39$, we obtain value of $\Omega_{m0} = 0.37$ ($\chi^2 = 96.25$). Another good fit can be obtained with marginalization over \mathcal{M} . In that case we obtain $\mathcal{M} = -3.37$, $\Omega_{m0} = 0.40$. We test our results for the sample of 54 supernovae (Perlmutter sample C) and we realize that no significant differences were obtained. Note that in our model the numerical value for Ω_{m0} is larger than in the standard approach with cosmological constant, where $\Omega_{m0} \approx 0.3$ ($\Omega_{m0} = 0.29$ for sample A and $\Omega_{m0} = 0.28$ for sample C [4]).

However, knowledge of the best-fit values alone has not sufficient scientific relevance, if confidence levels for parameter intervals are not presented too. Therefore, we carry out the model parameters estimation using the minimization procedure, based on the likelihood method. We could observe

that results obtained by this two methods are almost identical. At the confidence level of 68.3 % we obtain limits for values of parameters \mathcal{M} and Ω_{m0} separately for samples A and C (Table 2). For example for Perlmutter sample A (with marginalization over \mathcal{M}) we obtain that $\mathcal{M} = -3.37$ and $\Omega_{m0} = 0.39^{+0.10}_{-0.08}$ while for $\mathcal{M} = -3.39$ we have $\Omega_{m0} = 0.37^{+0.05}_{-0.05}$

Varying Ω_{m0} and \mathcal{M} we can find best-fit confidence regions in the $(\Omega_{m0}, \mathcal{M})$ plane for our Perlmutter supernovae sample. In Fig. 5 we plot two confidence regions corresponding to levels of 95.5 (outer line) and of 68.3 (inner line) respectively. Since \mathcal{M} is related to the absolute luminosity M and the Hubble constant H_0 (see relation (26)), knowing M we can estimate H_0 . For example assuming that $0.25 < \Omega_{m0} < 0.40$ (what is generally accepted) and $M = -19.32$ we find that $61.9 \text{ km/sMpc} < H_0 < 69.2 \text{ km/sMpc}$.

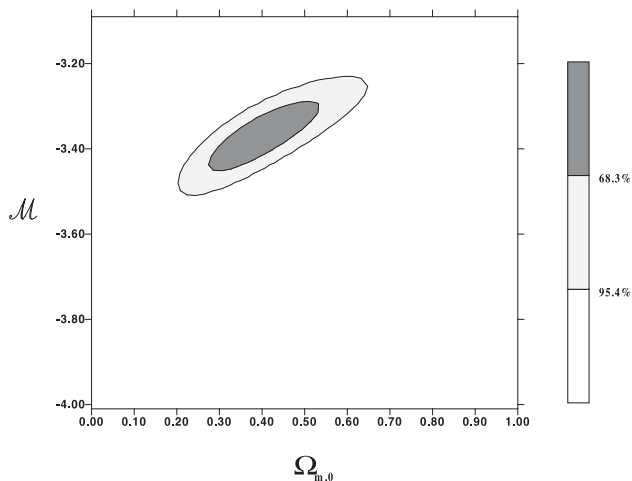


Figure 5: Confidence levels on the plane $(\Omega_{m0}, \mathcal{M})$. (Perlmutter Sample A). The figure shows of the preferred value of Ω_{m0} and \mathcal{M} at the confidence of level of 68.3 % and 95.4 %.

In Fig. 6 we show the levels of constant χ^2 on the plane $(\Omega_{m0}, \mathcal{M})$. In this procedure we find the minimal value of χ^2 , i.e., we consider best-fit values. The figure shows the preferred values of Ω_{m0} and \mathcal{M} .

For a deeper statistical analysis of the Stephani model in explaining the currently accelerating universe we consider 1D plot of the density distribution of $\Omega_{\text{non}0}$. From this analysis one can obtain the limits at the 1σ or 2σ level. Fig. 7 shows the density distribution for $\Omega_{\text{non}0}$ in the Stephani model. This distribution is obtained from the marginalization over \mathcal{M} . We obtain as a best fit value $\Omega_{\text{non}0} = 0.61$. One can conclude that at the confidence level of 68.3 % $\Omega_{\text{non}0} \geq 0.51$ and $\Omega_{\text{non}0} \leq 0.70$ while at the confidence level of 95.4 % we obtain that $\Omega_{\text{non}0} \in (0.41, 0.77)$. Fig. 8 shows the 1 dimensional density distribution for \mathcal{M} .

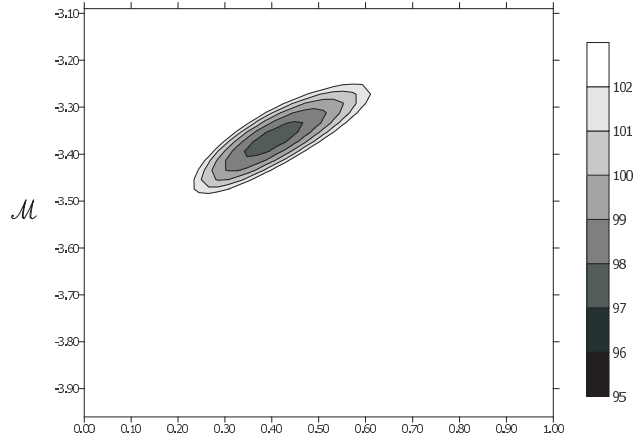


Figure 6: Levels of constant χ^2 on the plane $(\Omega_{m0}, \mathcal{M})$. The figure shows the preferred value of $(\Omega_{m0}, \mathcal{M})$.

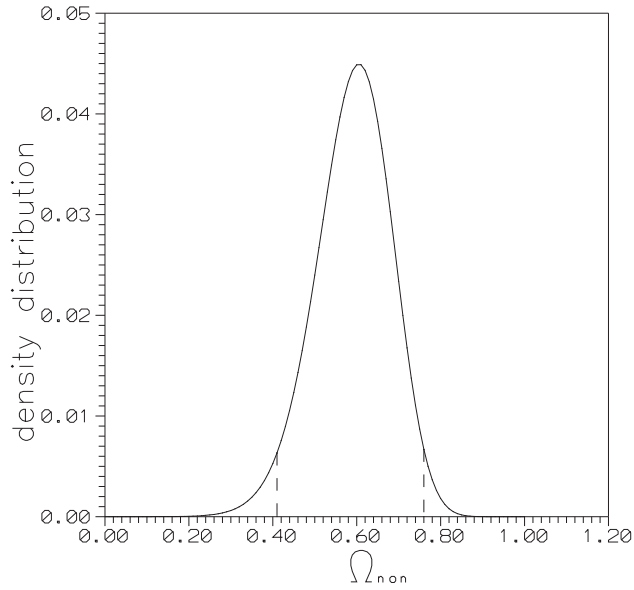


Figure 7: The density distribution for $\Omega_{\text{non}0}$ in the Stephani model (Perlmutter Sample A). $\Omega_{\text{non}0} > 0.41$, $\Omega_{\text{non}0} < 0.77$ at the confidence level of 95.4 %.

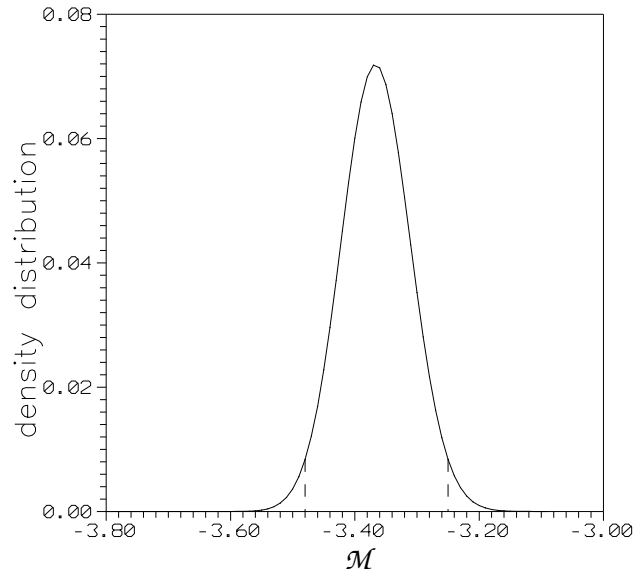


Figure 8: The density distribution for \mathcal{M} in the Stephani model (Perlmutter Sample A). The confidence level of 95.4 % is marked in the figure ($\mathcal{M} \in (-3.48, -3.25)$).

8 Statistical analysis with the Knop and Tonry samples.

Because the Perlmutter sample was completed four years ago, it would be interesting to use newer supernovae observations. Lately Knop *et al.* [7] have reexamined the Perlmutter sample with host-galaxy extinction correctly applied. They chose from the Perlmutter sample these supernovae which were the more securely spectrally identified as type Ia and have reasonable colour measurements. They also included eleven new high redshift supernovae and a well known sample with low redshift supernovae.

We have also decided to test our model using this new sample of supernovae. The mentioned authors distinguished few subsets of supernovae from this sample. We consider two of them. The first is a subset of 58 supernovae with extinction correction (Knop subsample 6; hereafter K6) and the second one a sample of 54 supernovae with low extinction (Knop subsample 3; hereafter K3). Sample C and K3 are similarly constructed because both contain only low extinction supernovae.

Another sample was presented by Tonry *et al.* [5] who collected a large number of supernovae published by different authors and added eight new high redshift SN Ia. This sample of 230 SNe Ia was recalibrated with con-

sistent zero point. Whenever it was possible the extinctions estimates and distance fitting were recomputed. However, none of the methods was able to apply to all supernovae (for details see Table 8 in [5]). This sample was improved by Barris who added 23 high redshift supernovae including 15 at $z \geq 0.7$ doubling the published number of object at this redshifts [6].

Despite of the mentioned above problems, the analysis of our model using this sample of supernovae could be interesting. We decide to analyse four subsamples. First, the full Tonry/Barris sample of 253 SNe Ia (hereafter sample TBa) is considered. The sample of 218 SNe Ia (hereafter sample TBb) consists of low extinction supernovae only (median V band extinction $A_V < 0.5$). Because the Tonry sample has a lot of outliers especially in low redshift, we separately analysed the sample where all low redshift ($z < 0.01$) supernovae are excluded. This sample again contains 218 SN Ia, but they are different than that belonging to the sample TBb (hereafter sample TBc). In the sample of 193 SN Ia all supernovae with low redshift and and high extinction are omitted (hereafter sample TBd).

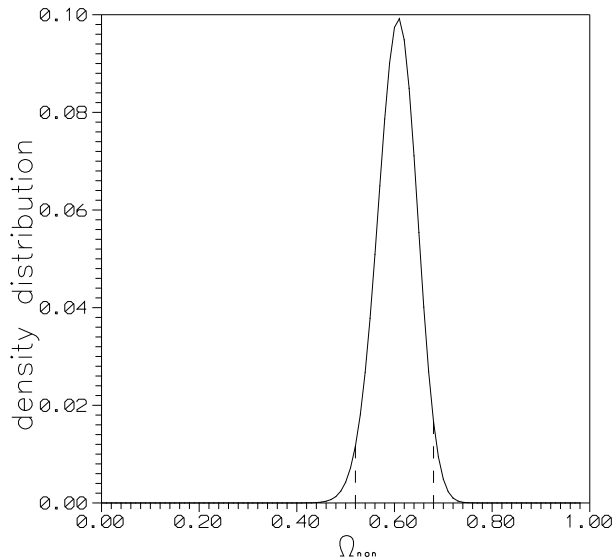


Figure 9: The density distribution for $\Omega_{\text{non}0}$ in the Stephani model (Tonry/Barris sample TBa). $\Omega_{\text{non}0} \in (0.52, 0.68)$ at the confidence level of 95.4 %.

Tonry and Barris [5, 6] presented redshift and luminosity distance observations for their sample of supernovae. Therefore, Eqs. (25) and (26) should be modified [19]:

$$m - M = 5 \log_{10}(\mathcal{D}_L)_{\text{Tonry}} - 5 \log_{10} 65 + 25 \quad (33)$$

and

$$\mathcal{M} = -5 \log_{10} H_0 + 25. \quad (34)$$

For $H_0 = 65 \text{ km s}^{-1} \text{ Mpc}^{-1}$ we obtain $\mathcal{M} = 15.935$.

The results obtained with the new sample is very similar to that obtained with Perlmutter sample but now errors decrease. The results with Tonry sample are almost identical to that with Perlmutter sample. For the sample TBa we obtain that $\Omega_{m0} = 0.39$, while for Λ CDM model $\Omega_{m0} = 0.32$ (for the sample TBd $\Omega_{m0} = 0.33$ [6]). Using Tonry sample we obtain at the confidence level of 95 % limit for $\Omega_{\text{non}} \in (0.52, 0.68)$ (see Fig. 9). However with the Knop sample we obtain the value Ω_{m0} more closed to value 0.3, what was obtained from CMBR and extragalactic data [20, 21], than in the previous case. However, it should be noted, that for Λ CDM model we obtain for the sample K3 $\Omega_{m0} = 0.25$ while for the sample K6 $\Omega_{m0} = 0.28$. It means, that our conclusion that the numerical value for Ω_{m0} in our model is larger than in the standard approach (Λ CDM model) is still valid.

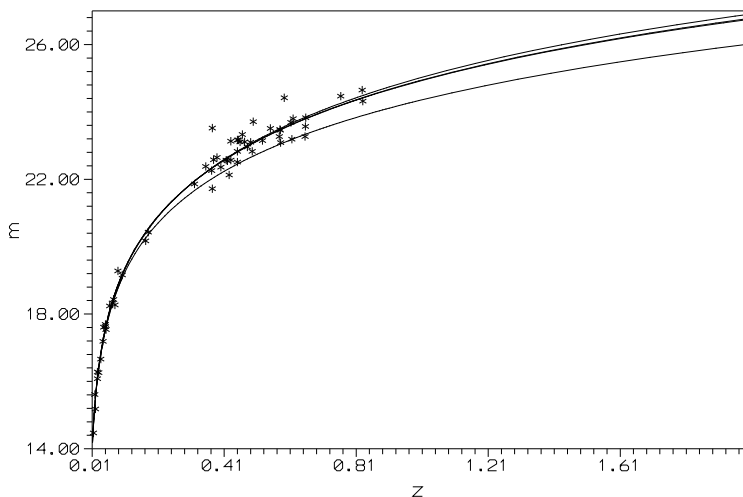


Figure 10: The Redshift-magnitude relation for the Stephani model (Knop Sample K3).

In Fig. 10 we present plots of redshift-magnitude relations for Stephani model Perlmutter sample A. The lower line corresponds to the standard Einstein-de Sitter model, the line in the middle to our spherically symmetric Stephani model, i.e. $\mathcal{M} = -3.46$, $\Omega_{m0} = 0.32$ (this line is inseparable from the Λ CDM model with $\Lambda = 0.75$ and $\Omega_{m0} = 0.25$), the upper line to Stephani model with $\Omega_{m0} = 0.25$. From Fig. 10 we can see that the Λ CDM model and our best fit model are indistinguishable also on the basis of the Knop sample.

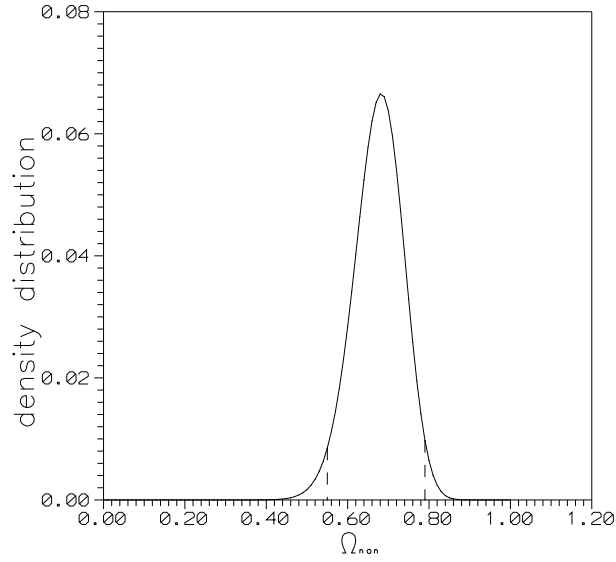


Figure 11: The density distribution for $\Omega_{\text{non}0}$ in the Stephani model (Knop sample K3). $\Omega_{\text{non}0} \in (0.55, 0.79)$ at the confidence level of 95.4 %.

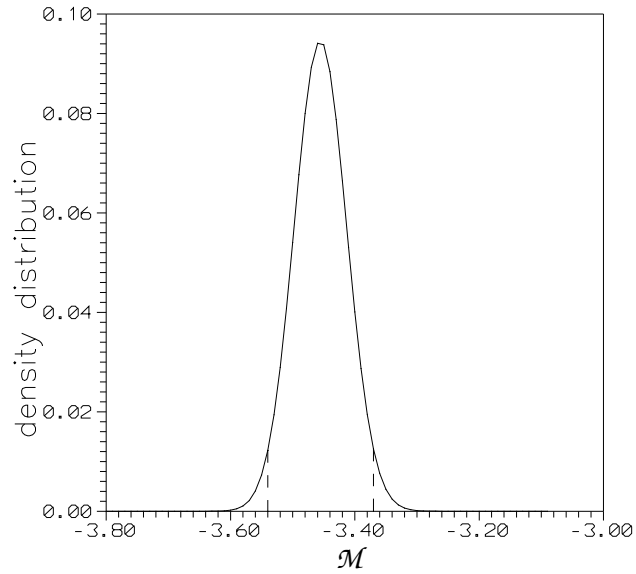


Figure 12: The density distribution for \mathcal{M} in the Stephani model (Knop Sample K3). $\mathcal{M} \in (-3.54, -3.37)$ at the confidence level of 95.4 %.

Using the Knop sample (Figs 11 and 12) we obtain $\Omega_{\text{non}} \in (0.55, 0.79)$ at the confidence level of 95 %. Because Knop discuss very carefully extinction correction and as a result his sample has extinction correctly applied, we think that using the limit obtained from the Knop's sample is the most appropriate. Our results show that Stephani model is consistent with SNIa data at the 95 % confidence level. Our study shows that Stephani model is very good fit to latest supernovae data and should be treated as a alternative to Λ CDM (Perlmutter) model.

9 CMB peaks in the Stephani model

The CMB peaks arise from acoustic oscillations of the primeval plasma. Physically these oscillations represent hot and cold spots. Thus, the wavelength of the perturbation which contributes the most to the density distribution at the time of the last scattering corresponds to a peak in the power spectrum. In the Legendre multipole space this corresponds to the angle subtended by the sound horizon at the last scattering epoch. Higher harmonics of the principal oscillations, which oscillated more than once, correspond to secondary peaks.

It is well known that the locations of the peaks are very sensitive to the variations in the parameters of the model. Therefore, it can be used as a sensitive probe to constraint the cosmological parameters and discriminate among various models.

The locations of the peaks are set by the acoustic scale l_A which can be defined in terms of an angle θ_A subtended by the sound horizon at the last scattering surface. In a general case calculation of the angle θ corresponding to acoustic or particle horizon existing at the recombination epoch is not an easy task even in the Friedmann model. One of the way to find θ is to solve an appropriate Euler-Lagrange problem ([22], [17]). If the angle θ_A is small (in general it is small, because $c_s \ll c$), hence the acoustic scale $l_A = \pi/\theta_A$ is given by

$$l_A = \pi \frac{\int_{x_{\text{dec}}}^1 dx/h(x)}{\int_0^{x_{\text{dec}}} c_s(x) dx/h(x)}, \quad (35)$$

where

$$h(x) = \sqrt{\Omega_{r0} + \Omega_{m0}x + \Omega_{\text{non}0}x^3} \quad (36)$$

and the relation between z and x is given by the equation (31). $c_s(x)$ is a speed of sound in the plasma and varies with the expansion (we assume additionally presence of radiation in the model and Ω_{r0} is an energy density parameter corresponding to radiation at the present epoch). Similarly Ω_{m0}

corresponds to nonrelativistic matter and $\Omega_{\text{non}0}$ to nonhomogeneity. The sound velocity can be calculated from the formula

$$c_s^2(x) = \frac{\frac{4}{3}\Omega_{r0} - \frac{2}{3}\Omega_{\text{non}0}x^3}{4\Omega_{r0} + 3\Omega_{m0}x + \Omega_{\text{non}0}x^3} \quad (37)$$

In the case without cosmological term the parameters Ω_{m0} and $\Omega_{\text{non}0}$ are not independent, and $\Omega_{\text{non}0}$ can be expressed as

$$\Omega_{\text{non}0} = 1 - \Omega_{r0} - \Omega_{m0}. \quad (38)$$

In the model of primeval plasma, there is a simple relation

$$l_m \approx l_A(m - \phi_m) \quad (39)$$

between the location of the m -th peak and the acoustic scale [23, 24]. The prior assumptions in our calculations are $\Omega_{r0} = 9.89 \cdot 10^{-5}$, $\Omega_{b0} = 0.05$ (baryonic matter energy density), and the spectral index for initial density perturbations is $n = 1$. Moreover we put for the present value of the Hubble parameter $H_0 = 65$ km/sMpc.

The phase shift is caused by the pre-recombination physics (plasma driving effect) and hence, is not significantly influenced by the Stephani term at that epoch. Therefore the phase shift ϕ_m can be taken from standard cosmology [24]

$$\phi_m \approx 0.267 \left[\frac{r(z_{\text{dec}})}{0.3} \right]^{0.1}, \quad (40)$$

where $\Omega_{b0}h^2 = 0.02$, $r(z_{\text{dec}}) \equiv \rho_r(z_{\text{dec}})/\rho_m(z_{\text{dec}}) = \Omega_{r0}/\Omega_{m0}x_{\text{dec}}$. Radiation energy is composed of two components: electromagnetic energy and neutrino energy $\Omega_{r0} = \Omega_{\gamma0} + \Omega_{\nu0}$, $\Omega_{\gamma0} = 2.48h^{-2} \cdot 10^{-5}$, $\Omega_{\nu0} = 1.7h^{-2} \cdot 10^{-5}$. $r(z_{\text{dec}})$ is the ratio of radiation to matter densities at the surface of last scattering.

In the Friedman models ($\Omega_{\text{non}0} = 0$) with possible presence of cosmological constant we obtain:

$$\begin{aligned} \Omega_{m0} = 1.0 \quad \Omega_{\text{non}0} = 0.: \quad & l_{\text{peak},1} = 203, l_{\text{peak},2} = 471, l_{\text{peak},3} = 739, \\ \Omega_{m0} = 0.3 \quad \Omega_{\Lambda} = 0.7: \quad & l_{\text{peak},1} = 225, l_{\text{peak},2} = 536, l_{\text{peak},3} = 847. \end{aligned}$$

The influence of $\Omega_{\text{non}0}$ on the location of the peaks results in shifting them towards higher values of l in comparison to the model with Ω_{r0} . For example, for $\Omega_{b0} = 0.05$, $h = 0.65$, the different choices of $\Omega_{\text{non}0}$ yield

$$\begin{aligned} \Omega_{m0} = 0.4 \quad \Omega_{\text{non}0} = 0.6: \quad & l_{\text{peak},1} = 212, l_{\text{peak},2} = 500, l_{\text{peak},3} = 789, \\ \Omega_{m0} = 0.3 \quad \Omega_{\text{non}0} = 0.7: \quad & l_{\text{peak},1} = 216, l_{\text{peak},2} = 514, l_{\text{peak},3} = 812. \end{aligned}$$

On the other hand from the Boomerang observations [26] we obtain $l_{\text{peak},1} = 200 \div 223$, $l_{\text{peak},2} = 509 \div 561$. We also compare the results from our model to recent bounds on the location of the first two peaks

obtained by WMAP experiment [27, 28]. Namely $l_{\text{peak},1} = 220.1 \pm 0.8$, $l_{\text{peak},2} = 546 \pm 10$, together with the bound of the location of the third peak obtained by Boomerang experiment $l_{\text{peak},3} = 825_{-13}^{+10}$ which lead to quite strong constraints on the model parameters. These constraints can be summarized as follows. The Stephani model is in agreement with observations and we conclude that the influence of the term $\Omega_{\text{non}0}$ is not very significant in our case. However, phase shift ϕ is taken from the standard cosmology, i.e., we assume that the contribution from the "Stephani nonhomogeneity" is insignificant at the pre-recombination epoch. If this assumption is not valid then the limit from CMB will change.

It should be also noted that the Big-Bang Nucleosynthesis (BBN) is a very well tested area of cosmology and does not allow for significant deviation from the standard expansion law, apart from very early times before the onset of the BBN. The consistency with the BBN seems to be necessary in the Stephani model. We consider only non-relativistic matter ρ in the Stephani model. In this case we could approximate that $\Omega_{\text{non}0}$ term scales like $(1+z)$. It is clear that the contribution of the "Stephani nonhomogeneity term" cannot dominate over the standard radiation term before the onset of BBN, i.e., for $z \cong 10^8$ and as a result has no effect on the BBN.

10 Conclusions

Our investigations show that the Stephani model is an excellent fit to both Perlmutter data points and currently available Knop's data points. Summarizing, relatively large value of $\Omega_{\text{non}0} = 0.61_{-0.10}^{+0.08}$ can explain supernovae data of Perlmutter. In the range of observed redshifts of supernovae ($z < 1$) the curve corresponding to $m - z$ relation in our model is almost indistinguishable from the Λ CDM (Perlmutter) model with cosmological constant. With future data from SNAP the error bars in the estimation of the model parameters will be reduced significantly. Together with new limits for $\Omega_{m,0}$ (obtained from extragalactic data) it will be possible discriminate between Stephani model and Λ CDM (Perlmutter) model.

Locally our spherically symmetric Stephani universe is indistinguishable from the Friedman one (the same equation of state, the same local geometry), hence local physical cosmology in both models must be the same. In other words standard scenario of the evolution of the universe remains valid. Especially in the early universe effects of non-homogeneity become negligible. This is easily seen if we evaluate the energy density parameter Ω_α for matter

as a function of the scale factor R

$$\Omega_\alpha(R) = \frac{1}{1 - 3\beta C_\alpha R^{2+3\alpha}}. \quad (41)$$

In the early universe relativistic matter dominates ($\alpha = 1/3$) and from the above relation it follows that $\Omega_\alpha(R)$ tends very quickly to 1 for $R \rightarrow 0$. It means that $\Omega_{\text{non}}(R) \rightarrow 0$. This justifies application of standard physical cosmology (including e.g. primordial nucleosynthesis) for our nonhomogeneous model.

Freese and Lewis in [29] have recently proposed interesting alternative model explaining the currently accelerating Universe. In this model which is called the Cardassian model the standard Friedmann-Robertson-Walker (FRW) equation is modified by the presence of an additional term ρ^n , namely

$$H^2 = \frac{\rho}{3} + B\rho^n, \quad (42)$$

where ρ is a total energy density (matter + radiation), and B is a positive constant. This proposal seems to be attractive because the expansion of the universe is accelerated automatically due to the presence of the additional term (if we put $B = 0$ then the standard FRW equation is recovered) without postulating existence of unknown form of dark energy.

Note that putting $\rho \equiv 3\rho_{m0}/R^3$ (and hence $\alpha \equiv 0$) and $n = 1/3$ and $B \equiv -3\beta/\sqrt{3\rho_{m0}}$ the above equation could be rewritten in the form:

$$H^2 = \frac{\rho}{3} + B\rho^n = \frac{\rho_{m0}}{R^3} + \frac{(-3\beta)}{R}. \quad (43)$$

Comparing to (1) we realize that we obtain correspondence between Cardassian and Stephani models.

When for simplicity we assume that the energy density parameter for radiation matter vanishes ($\Omega_{r0} = 0$) we recover the model analysed in our previous paper [30]. We note that considered by us spherically symmetric Stephani model is a special realization or in other words is dynamically equivalent to the Cardassian model for $n=1/3$. It is interesting that this value of n parameter is reasonable from the observational joint test analysis of both CMB from and SNIa [31].

Let us note that in our model there is the cosmic coincidence problem, i.e. problem why did the nonhomogeneity start to dominate the present evolution of the Universe only fairly recently? There is no satisfactory solution of this problem and some other face of fine tuning coincidence is required.

References

- [1] Jakacka I and Stelmach J 2001 *Class. Quantum Grav.* **18** 2643
- [2] Krasinski A 1985 *GRG* **15** 673
- [3] Krasinski A 1997 *Inhomogeneous Cosmological Models* Cambridge University Press Cambridge 1997 p.317
- [4] Perlmutter S *et al.* 1999 *Astrophys. J.* **517** 565
- [5] Tonry J L *et al.* 2003 *Astrophys. J.* **594** 1, astro-ph/0305008
- [6] Barris B J *et al.* 2003 astro-ph/0310843
- [7] Knop R A *et al.* 2003, astro-ph/0309368
- [8] Perlmutter S *et al.* 1998 *Nature* **391** 51, Perlmutter S *et al.* 1999, *Astrophys. J.* **517** 565, Garnavich P M *et al.* 1998 *Astrophys. J. Lett.* **493** L53, Riess A G *et al.* 1998 *Astron. J.* **116** 1009
- [9] Caldwell R R, Dave R and Steinhardt P J, 1998 *Phys. Rev. Lett.* **80** 1582, Zlatev I, Wang L and Steinhardt P J, 1999 *Phys. Rev. Lett.* **82** 896, Steinhardt P J, Wang L and Zlatev I 1999 *Phys. Rev.* **D59** 123504
- [10] Dąbrowski M P and Stelmach J, in *Large Scale Structure in the Universe* IAU Symposium No 130 eds. Jean Adouze, Marie-Christine Palletan and Alex Szalay, (Kluwer Academic Publishers, 1988), 566.
- [11] Dąbrowski M P and Stelmach 1987 *J Astron. Journ.* **93** 1373
- [12] Stelmach J, Dąbrowski M P and Byrka R 1993 *Nuclear Physics* **B406** 471
- [13] Celerier M N 2003 *Astronomy and Astrophysics* **353** 63
- [14] Dąbrowski M P and Stelmach J 1986 *Ann. Phys (N.Y.)* **166** 422
- [15] Szydlowski M, Krawiec A and Dąbrowski M P 2002 *Phys. Rev* **D66** 064003
- [16] Dąbrowski M P and Hendry M A 1998 *Astrophys. J.* **498** 67
- [17] Weinberg S 1972 *Gravitation and Cosmology* (Wiley, New York, 1972)
- [18] Riess A G 1998 *Astron. J.* **116** 1009

- [19] Williams B F *et al.* 2003 astro-ph/0310432
- [20] Peebles P J E, Ratra B 2003 *Rev. Mod. Phys.* **75** 559, astro-ph/0207347
- [21] Lahav O 2002 astro-ph/0208297
- [22] Narlikar J V 1983 *Introduction to Cosmology*, (Jones and Barlett, Boston 1983)
- [23] Doran M, Lilley M, Schwindt J and Wetterich C 2001 *Astrophys. J.* **559** 501
- [24] Hu W, Fukugita M, Zaldarriaga M and Tegmark M 2001 *Astrophys. J.* **549** 669
- [25] Ichiki K, Yahiro M, Kajino T, Orito M and Mathews G J 2002 *Phys. Rev. D* **66** 043521
- [26] de Bernardis P *et al.* 2002 *Astrophys. J.* **564** 559
- [27] Spergel D N *et al.* 2003, astro-ph/0302209.
- [28] Page L *et al.* 2003, astro-ph/0302220
- [29] Freese K and Lewis M 2002 *Phys. Lett. B* **540**1, astro-ph/0201229
- [30] Godłowski W, Szydlowski M and Krawiec A 2004 accepted for publication in *Aastrophys. J.*, astro-ph/0309569
- [31] Sen S 2003 AA588 1 astro-ph/0211634

Table 1: Results of the statistical analysis of the model using the best fit with minimum χ^2 (denoted by BF). The case in which we marginalize over \mathcal{M} is denoted by \mathcal{M} .

sample	Ω_{m0}	$\Omega_{\text{non}0}$	\mathcal{M}	χ^2	method
A	0.37	0.63	-3.39	96.3	BF
	0.40	0.60	-3.37	96.1	\mathcal{M} , BF
C	0.36	0.64	-3.42	53.4	BF
	0.36	0.64	-3.42	53.4	\mathcal{M} , BF
K3	0.29	0.71	-3.48	61.3	BF
	0.32	0.68	-3.46	61.0	\mathcal{M} , BF
K6	0.36	0.64	-3.53	56.3	BF
	0.36	0.64	-3.51	56.0	\mathcal{M} , BF
TBa	0.38	0.62	15.905	262.3	BF
	0.39	0.61	15.915	262.2	\mathcal{M} , BF
TBb	0.39	0.61	15.925	204.8	BF
	0.39	0.61	15.925	204.8	\mathcal{M} , BF
TBc	0.39	0.61	15.915	229.3	BF
	0.41	0.59	15.925	229.2	\mathcal{M} , BF
TBd	0.39	0.61	15.925	192.7	BF
	0.39	0.61	15.925	192.7	\mathcal{M} , BF

Table 2: Results of the statistical analysis of the model using the likelihood method (denoted by L). The case in which we marginalize over \mathcal{M} is denoted by \mathcal{LM} .

sample	Ω_{m0}	\mathcal{M}	method
A	$0.37^{+0.05}_{-0.05}$	-3.39	L
	$0.39^{+0.10}_{-0.08}$	$-3.39^{+0.06}_{-0.05}$	\mathcal{LM}
C	$0.36^{+0.05}_{-0.05}$	-3.42	L
	$0.36^{+0.10}_{-0.08}$	$-3.42^{+0.05}_{-0.05}$	\mathcal{LM}
K3	$0.29^{+0.04}_{-0.03}$	-3.48	L
	$0.29^{+0.06}_{-0.06}$	$-3.46^{+0.05}_{-0.04}$	\mathcal{LM}
K6	$0.31^{+0.06}_{-0.06}$	-3.53	L
	$0.33^{+0.08}_{-0.07}$	$-3.51^{+0.03}_{-0.03}$	\mathcal{LM}
TBa	$0.38^{+0.03}_{-0.03}$	15.905	L
	$0.39^{+0.04}_{-0.04}$	$15.915^{+0.02}_{-0.02}$	\mathcal{LM}
TBb	$0.39^{+0.03}_{-0.03}$	15.925	L
	$0.39^{+0.04}_{-0.04}$	$15.925^{+0.02}_{-0.02}$	\mathcal{LM}
TBc	$0.39^{+0.02}_{-0.02}$	15.915	L
	$0.40^{+0.04}_{-0.04}$	$15.925^{+0.02}_{-0.02}$	\mathcal{LM}
TBd	$0.39^{+0.03}_{-0.03}$	15.925	L
	$0.39^{+0.04}_{-0.04}$	$15.935^{+0.02}_{-0.02}$	\mathcal{LM}